MIJST
MIST International Journal of Science and Technology

Correlation Analysis of Rate of TEC Index and Spread F over North American Ionosondes

Mehdi Hasan Rafi* and Md Golam Mostafa

Department of Electrical Electronic and Communication Engineering, Military Institute of Science and Technology (MIST), Dhaka-1216, Bangladesh

Corresponding Email: *rafimehdihasan@gmail.com*

ARTICLE INFO

Article History:

Received:14th April 2025
Revised:26th May 2025
Accepted: 01st June 2025
Published: 30th June 2025

Keywords:

GNSS-TEC
Ionospheric irregularities
ROTI
Spread F
TID

ABSTRACT

This study investigates the diurnal, seasonal, and latitudinal variations of Spread F and the Rate of TEC Index (ROTI) over North America during the high solar activity period of 2014. Using GNSS-based ROTI measurements and Digisonde ionograms from multiple stations, we systematically analyze the relationship between Spread F occurrences and ROTI enhancements. The analysis incorporated Diurnal and seasonal variations to determine dominant trends and potential driving mechanisms, such as medium-scale traveling ionospheric disturbances (MSTIDs) and polarization electric fields. Seasonal and latitudinal variations of Spread F occurrences and ROTI fluctuations are found to be strongly linked to MSTIDs and geomagnetic activity. A clear seasonal dependence was observed at the stations situated under the transitional and mid-latitude regions of the ionosphere. The maximum irregularity occurred in April for transitional region stations and in November for mid-latitudinal stations. Additionally, Spread F and ROTI exhibit similar diurnal and seasonal trends, with maximum irregularity occurrences during nighttime (20:00–02:00 LT). A distinct seasonal dependence is observed, with transitional region stations peaking in winter and mid-latitude stations in summer. Notably, spread F was consistently associated with notable ROTI values (>0.15 TECU/min), suggesting gravity waves and polarization electric fields as driving mechanisms. Through detailed case studies, we demonstrated that MSTIDs, likely driven by gravity wave dynamics, play a crucial role in generating plasma irregularities, which in turn enhance ROTI values and contribute to Spread F formation. Under quiet geomagnetic conditions, these irregularities exhibit a strong daytime preference. Conversely, during disturbed geomagnetic conditions (e.g., the geomagnetic storm), the spatial extent of ionospheric irregularities increased significantly, affecting both transitional and mid-latitude stations for both daytime and nighttime. By demonstrating a persistent relationship between Spread F and ROTI, this study advances ionospheric modelling efforts and supports the development of improved space weather forecasting techniques, crucial for GNSS-based navigation and communication systems.

1. INTRODUCTION

The ionosphere, a region of the Earth's upper atmosphere extending from approximately 60 km to 1000 km, plays a crucial role in radio wave propagation and satellite communication. However, ionospheric irregularities, caused by density gradients and plasma instabilities, can lead to rapid fluctuations in the amplitude and phase of trans-ionospheric signals. These irregularities are especially prevalent at low latitudes and near the magnetic equator, affecting Global Navigation Satellite System (GNSS) signals, radar applications, and radio communications (Kelley, 2009). Equatorial plasma bubbles (EPBs) and Spread F are two primary forms of ionospheric irregularities, with EPBs spanning several kilometers and Spread F consisting of smaller-scale plasma structures.

The spread F is classified into four types based on the shape of diffusion on the ionogram: a) Frequency Spread F (FSF), b) Range Spread F (RSF), c) Mixed Spread F (MSF), and d) Branch Spread F (BSF) (Davies et al., 1990). However, FSF is inherently rarer compared to RSF, particularly in low and mid latitudes, because it is often associated with smaller-scale plasma irregularities that do not extend over long distances along magnetic field lines (Maruyama & Matuura, 1984; Abdu, 2001). FSF events tend to occur in the bottomside F-

layer under conditions of weaker instability growth, making them less likely to evolve into large-scale depletions that cause significant signal disruptions (Tsunoda, 1985). Additionally, FSF's visual classification is more ambiguous than RSF's, especially in mid-latitude ionograms, where spread characteristics may be subtle and easily confounded with noise or other irregularities. This introduces greater classification uncertainty, which can compromise the robustness of quantitative analysis.

Basu & Kelley (1979) analyzed the formation and evolution of EPBs using radar observations in the American sector, concluding that ionospheric disturbances were linked to equatorial electrodynamics and plasma instabilities. Aarons et al. (1980) studied seasonal and longitudinal variations using satellite beacon data, highlighting how solar activity influences EPB occurrences. These early studies established the foundation for subsequent research into ionospheric irregularities worldwide.

Research on ionospheric irregularities has been conducted extensively across various geographic regions. Das Gupta et al. (1981) and Chakraborty et al. (1999) investigated ionospheric irregularities in the Indian sector using ionosonde and scintillation data to understand plasma instability mechanisms. Their studies emphasized the role of post-sunset ionospheric dynamics in irregularity formation. Chandra et al. (2003) expanded on these findings by analyzing ionosonde data to show latitudinal variations in Spread F characteristics. Huang (1970, 1985, 1987) explored the development of Spread F in the western Pacific sector, focusing on the role of geomagnetic activity and atmospheric waves using ground-based and satellite observations. These studies confirmed that ionospheric disturbances exhibit regional and seasonal dependencies. In the Brazilian and African sectors, Mullen et al. (1985) and D'ujanga et al. (2018) analyzed Spread F occurrence using GNSS and ionosonde data, demonstrating the impact of solar cycle variations on irregularity formation and the variability of plasma bubbles in different magnetic environments.

Pi et al. (1997) defined the Rate of TEC Index (ROTI) as the standard deviation of the rate of TEC (ROT) over a 5-minute interval, providing a method for estimating ionospheric irregularities using GPS receivers. One key advantage of ROTI over the scintillation index S4, which requires high-rate GNSS signals for computation, is that ROTI can be derived from standard dual-frequency observations at a 30-second sampling rate. Based on the findings of Pi et al. (1997) and Basu et al. (1999), ROTI has been widely used as a proxy for detecting ionospheric irregularities. Although numerous studies have focused on ROTI characteristics, especially in equatorial and high-latitude ionospheric regions (Kotulak et al., 2020; Cherniak et al., 2014, 2018), fewer studies have examined mid-latitude irregularities. The development of ROTI maps based on an extensive network of permanent GNSS stations has significantly improved the ability to study ionospheric irregularities on both regional and global scales (Cherniak et al., 2018). Compared to polar and equatorial regions, the mid-latitude ionosphere is generally less affected by ionospheric disturbances (Kintner et al., 2013).

Nighttime ionospheric scintillations observed in GNSS trans-ionospheric links, resulting from irregular plasma structures, have been reported, particularly during geomagnetic disturbances (Vadakke et al., 2017). The mid-latitude nighttime F-region often exhibits diffused plasma structures that persist from minutes to hours, commonly referred to as mid-latitude spread F (Berkner & Wells, 1934; Bowman, 1991, 1998). These irregularities arise due to spatial variations in electron density and can have significant implications for radio wave propagation. Wang et al. (2014) demonstrated a strong correlation between intense range spread F and scintillation events, highlighting the impact of these irregularities on communication and navigation systems.

Previous research has primarily focused on high-latitude ionospheric disturbances. Using data collected from more than 700 ground-based GPS stations, Cherniak et al. (2014, 2018) analyzed ROTI variations across high and mid-latitude regions of the Northern Hemisphere, revealing a distinct seasonal pattern in ionospheric irregularities. Perkins (1973) introduced the Perkins instability theory to explain mid-latitude Spread F formation, but later studies, such as Zakharenkova et al. (2016), showed that additional mechanisms, including traveling ionospheric disturbances (TIDs) and atmospheric gravity waves, contribute to irregularity formation. These findings suggest that ionospheric irregularities at mid-latitudes result from a complex interplay of electrodynamic and neutral atmospheric processes. Perkins instability alone does not sufficiently account for the development of mid-latitude spread F. However, research by Huang et al. (1994) and Miller et al. (1997) has shown that the presence of gravity waves and related disturbances in the electric field near the lower ionospheric region can considerably enhance the instability's growth rate. Previous studies by Bowman and Monro (1988) and Otsuka et al. (2009) have determined a correlation between MSTIDs and mid-latitude spread F. Furthermore, research by Narayanan et al. (2018), Otsuka et al. (2007), and Yokoyama et al. (2009) have demonstrated that the coupling between the E and F regions plays a crucial role in generating and sustaining MSTIDs, further influencing the development of mid-latitude ionospheric irregularities.

Recent studies in Europe have provided new insights into the correlation between ROTI and Spread F, particularly in the mid-latitude region. Paul et al. (2024) analyzed the diurnal, seasonal, and latitudinal variations of ROTI occurrence using digisonde and GNSS data across multiple European stations, finding a strong correlation between ROTI and Spread F. The highest frequency of irregularities was detected near 45°N latitude, occurring predominantly between 18:00 and 05:00 UT, with peak seasonal activity noted in January. In contrast, at lower mid-latitude Digisonde locations (latitudes below 45°N), the irregularities were most commonly recorded from 19:00 to 04:30 UT during the month of July. Cherniak et al. (2014, 2018) presented ROTI maps for the European mid-latitude ionosphere, demonstrating that ionospheric disturbances in this region are influenced by geomagnetic activity and lower atmospheric forcing. Pi et al. (1997) introduced ROTI as a reliable GNSS-based index for identifying ionospheric irregularities, later adopted by the

International GNSS Service (IGS) for global monitoring (Cherniak et al., 2018). Their research showed that ROTI effectively tracks the intensity and distribution of ionospheric irregularities and is particularly useful for identifying space weather effects on navigation systems.

A long-term comparative analysis of nighttime spread F events at two mid-latitude stations in Europe, separated by roughly 20° in latitude, over an entire solar cycle, demonstrated notable differences in spread F frequency between the sites (Paul et al., 2022). Expanding on this, recent statistical investigations have examined spread F characteristics at eight mid-latitude European Digisonde stations for selected years: 2017, 2020, and 2021 (Paul et al., 2023). Prior work has also explored the influence of MSTIDs and the variety of ionogram features linked to spread F evolution (Paul et al., 2019; Paul et al., 2021). The study assessed both temporal and longitudinal variations in ionospheric irregularities across Europe by focusing on elevated ROTI values (greater than 0.15 TECU/min) recorded at eight Digisonde sites during 2011. Notably, previous studies (Yang and Liu, 2016) have established a strong relationship between such ROTI enhancements and occurrences of amplitude (S4) and phase scintillation, suggesting that F-region irregularity structures emerge when ROTI crosses this threshold.

In Asia, Lee et al. (2009) and Zhang et al. (2015) examined ionospheric disturbances with GPS TEC measurements, assessing latitudinal differences in irregularity strength and their correlation with geomagnetic storms. In a recent study, Hong et al. (2024) provided the first reported measurements of Spread F and ROTI occurrence rates over Vietnam, focusing on regions near the equatorial ionization trough and the northern crest of the equatorial ionization anomaly within the Asian longitudinal sector. Their findings indicate that Spread F events reach their highest monthly frequencies in April, with a diurnal peak occurring between approximately 21:15 and 23:15 LT.

Despite extensive research in Asia and Europe, a significant gap remains in studying ionospheric irregularities over North America using combined GNSS and ionosonde data. Direct investigations of ROTI and Spread F in this region are rare, underscoring the need for geographically targeted, integrated analyses. While ROTI has been well-documented during storm events, its connection to Spread F remains underexplored. Key mechanisms driving these correlations, such as MSTIDs, require further investigation, particularly for mid-latitude irregularities. To date, no comprehensive study has examined the simultaneous occurrence of Spread F and ROTI across North America, especially in transitional and mid-latitude regions. The present study addresses this gap by systematically analyzing ionospheric irregularities over North America during 2014, a representative year of peak solar activity during solar cycle 24.

Using Digisonde and GNSS data from multiple American stations, it explores the diurnal, seasonal, and latitudinal variations of ROTI, revealing a strong correlation with Spread F. By integrating both datasets, this research provides new insights into the spatiotemporal characteristics of ionospheric disturbances, enhancing the understanding and forecasting of space weather effects on communication and navigation systems. Additionally, case studies from both geomagnetically quiet and disturbed periods offer a comprehensive perspective on ionospheric dynamics. The findings will serve as a foundation for future research, improving ionospheric models and space weather prediction tools for the North American sector.

2. DATA AND METHODS

This investigation makes use of Digisonde ionograms sourced from the Digital Ionogram Database (DIDBase), hosted by the Global Ionospheric Radio Observatory (GIRO) portal, with data resolution details outlined in Table 1. Additionally, we incorporate d-TEC and ROTI maps for North America. These resources enable a detailed examination of ionospheric irregularities in both transitional and mid-latitude regions, focusing particularly on MSTIDs and Spread F events. The d-TEC and ROTI datasets are derived from the DRAWING-TEC (Dense Regional and Worldwide International GNSS-TEC Observation) project, offering 10-minute temporal resolution. The DRAWING-TEC initiative delivers fine-scale GNSS-based TEC mapping both globally and regionally (Yang et al., 2016). Specifically, d-TEC maps highlight perturbations in TEC, while ROTI maps indicate the intensity of phase fluctuations due to ionospheric irregularities. a representative year of peak solar activity during solar cycle 24. To examine the influence of geomagnetic activity on ionospheric irregularities, we incorporated the hourly Dst index data from the Kyoto University website https://aer-nc-web.nict.go.jp/GPS/DRAWING-TEC/tec_index.html.

Table 1. Summary of Digisonde Station Information and Ionogram Coverage in 2014

Station Name	Station Code	Geographic Latitude (°N)	Geographic Longitude (°W)	Geomagnetic Latitude (°N)	Sampling Interval
Idaho National Lab	IF843	43.81	112.68	54.1	15 min
Boulder	BC840	40.01	105.3	48.7	15 min
Alpena	AL945	45.07	83.56	53.3	15 min
Millstone Hill	MHJ45	42.6	71.5	51.0	02 min
Wallops Is	WI973	37.9	75.5	46.0	05 min
Melrose	ME929	29.71	82.0	38.4	15 min
Eglin	EG931	30.5	86.5	38.3	15 min
Austin	AU930	30.4	96.7	37.0	05 min

2.1 GPS IGS TEC Map Products

In this study, ionospheric irregularities over North America were investigated by analyzing the temporal and zonal distribution of significant ROTI activity (ROTI > 0.15 TECU/min) observed across eight Digisonde stations during 2014. The ROTI threshold of 0.15 TECU/min was selected based on its consistent usage in the prior literature as a baseline for detecting moderate ionospheric irregularities (Nguyen et al., 2021; Monte-Moreno et al., 2022). While thresholds vary by latitude due to differences in irregularity intensity, this intermediate value offers a balanced compromise suitable for broad regional analysis. Specifically, higher thresholds (e.g., >0.5 TECU/min) are commonly applied in low-latitude studies to isolate intense scintillation events, whereas lower thresholds (e.g., ~0.1 TECU/min) are often used in high-latitude contexts to capture more transient, weaker disturbances. In contrast, the 0.15 TECU/min threshold provides sufficient sensitivity to detect.

To explore the simultaneous occurrence of ROTI enhancements and Spread F phenomena, we examined ROTI maps generated by the DRAWING-TEC project, utilizing data with a temporal resolution of 10 minutes. These ROTI maps are constructed from slant values derived using carrier phase measurements collected from roughly 800 dual-frequency GPS receivers distributed throughout North America, operating at a 30-second sampling rate. To reduce cycle slips, data from satellites at elevation angles below 35° were excluded. The selected slant TEC values were then multiplied by a slant factor to derive vertical TEC estimates. The Rate of TEC (ROT) is calculated by Pi et al. (1997):

$$ROT = \frac{TEC_i^k - TEC_i^{k-1}}{t_k - t_{k-1}} \quad (1)$$

where *i* represents the satellite, and *k* denotes the time epoch. The Rate of the TEC Index (ROTI) is computed as the standard deviation of the detrended rate of TEC change by Pi et al. (1997):

$$ROTI = \sqrt{< ROT^2 > - < ROT >^2} \quad (2)$$

Detrended TEC (d-TEC) highlights fluctuations in TEC relative to the background TEC and is obtained by subtracting a 1-hour running average from the TEC time series. These fluctuations include both spatial and temporal variations (Paul et al., 2018 Shimazaki et al., 1962). The precision of relative TEC changes is estimated to be 0.01–0.02 TECU (1 TECU = 10^{16} m^{-2}), corresponding to ~1% of GPS signal wavelengths. For the DRAWING-TEC project, ROTI and d-TEC values are mapped at a 300 km ionospheric shell altitude, using a grid resolution of 0.15° × 0.15° in latitude and longitude (Otsuka et al 2013). To mitigate data sparsity, values were temporally smoothed with a 10-minute running average. The datasets used in this study include ROTI and d-TEC maps covering North America between 70° to 115° west longitude and 30° to 45° north latitude.

2.2 Digisondes Over North America

The ROTI threshold of 0.15 TECU/min was selected based on its consistent usage in the prior. In 2014, a network of Digisonde stations across North America was operational, providing ionograms essential for Spread F analysis. Eight of these stations were selected based on data availability, and their locations, coordinates, and sampling intervals are summarized in Table 1. These ionograms, available from DIDBase, were used to examine Spread F characteristics and their correlation with ROTI fluctuations. Figure 1 illustrates the geographic distribution of these Digisonde stations. Since ionospheric studies rely primarily on geomagnetic latitude rather than geographic latitude, we also include the geomagnetic latitude of Digisonde stations in Table 1.

This study provides a comprehensive assessment of transitional and mid-latitude ionospheric irregularities over North America by integrating Digisonde ionograms, ROTI maps, d-TEC data, and geomagnetic indices (Reinisch et al., 2011). By analyzing Spread F occurrences and their correlation with phase fluctuations in GPS signals, we aim to enhance the understanding of ionospheric disturbances in this region.

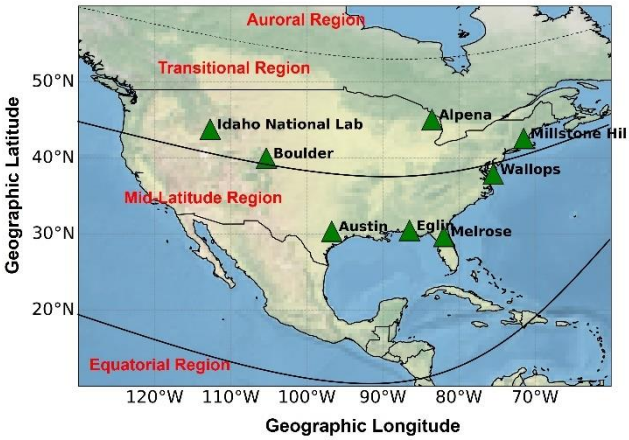

Figure 1: Map showing the geographical coordinates of the Digisonde stations (marked as triangles) over North America. Auroral, transitional, mid-latitude, and equatorial ionospheric regions are demarcated with geomagnetic latitude lines (marked as black)

3. RESULTS AND DISCUSSION

3.1 Diurnal Variation

Figure 2 presents a diurnal variation in the ROTI occurrences associated with RSF across Digisonde stations over North America for the year 2014. The Figure is divided into geomagnetically quiet days (blue bars) and disturbed days (brown bars). The panels represent data from (a) Idaho (LT = UT-8h), (b) Boulder (LT = UT-7h), (c) Alpena (LT = UT-5h), (d) Millstone (LT = UT-5h), (e) Wallops (LT = UT-5h), (f) Melrose (LT = UT-5h), (g) Eglin (LT = UT-5h), and (h) Austin (LT = UT-6h). Overlaid horizontal black and red curves indicate UT times of sunrise and sunset, respectively, while vertical gray bars denote data gaps.

The ROTI with RSF activity is most prominent during March–April and October–November at Idaho, Boulder, and Alpena, particularly under disturbed conditions. Idaho shows consistently high activity across both quiet and disturbed periods, while stations like Eglin and Austin exhibit low RSF occurrences, mostly during spring and fall equinoxes. From Figure 2(a)–(h) during the year 2014, RSF occurrences associated with ROTI are prominently observed across all eight stations, particularly between 20:00 and 02:00 LT. Over

Idaho (Figure 2a), significant RSF activity is evident mainly between 21:00 and 02:00 LT, with strong cases occurring during both equinoxes. A similar pattern is observed over Boulder (Figure 2b), where RSF signatures are noted between 21:30 and 02:30 LT, predominantly under quiet geomagnetic conditions. The Alpena station (Figure 4c) shows RSF events primarily during 23:00–03:00 LT in the second half of the year, although early months are marked by substantial data gaps. Over Millstone (Figure 2d), despite large data gaps from January to August, detectable irregularities between 01:00 and 04:00 LT are found from September to November. At Wallops (Figure 2e), RSF signatures appear mainly from 23:30 to 04:00 LT in March and October, with fewer detections during the mid-year months. Melrose (Figure 2f) exhibits a clear concentration of RSF cases between 00:00 and 05:00 LT in the post-equinoctial season. For Eglin (Figure 2g), limited events are seen during quiet geomagnetic periods, typically between 01:00 and 04:00 LT, while Austin (Figure 2h) shows weak RSF activity within a narrower window of 00:30 to 02:30 LT.

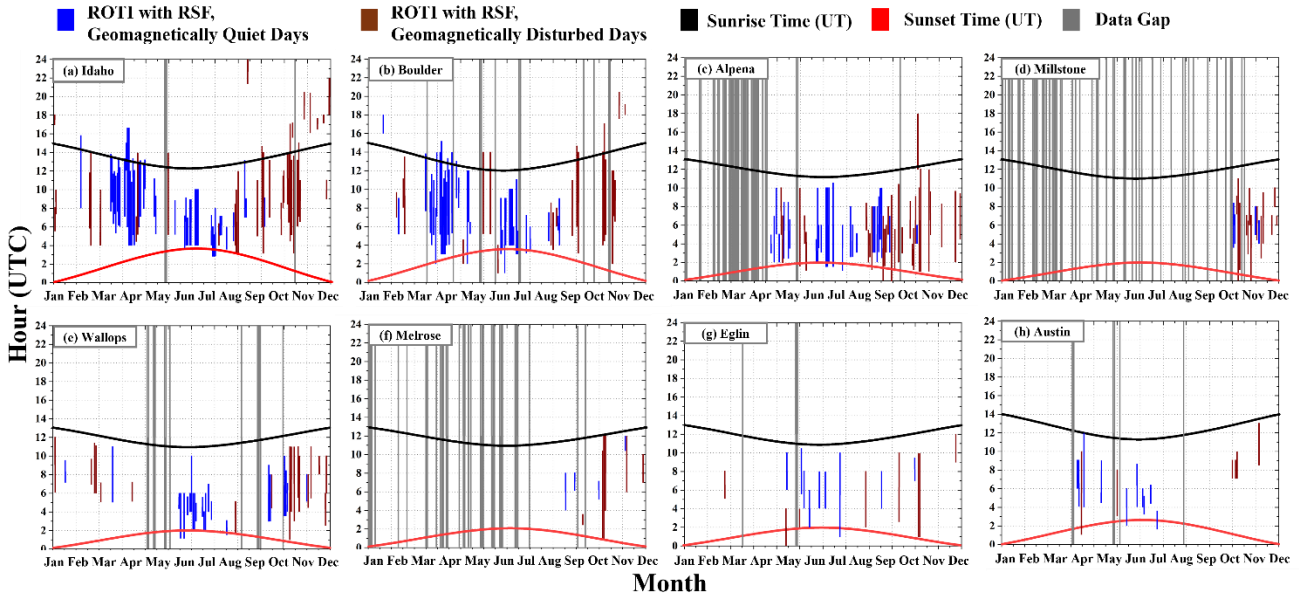

Figure 2: Diurnal Variation of ROTI Events in Association with Spread F across Digisonde stations over North America during 2014

It is also important to note the spatial distribution of the analyzed stations as displayed in Figure 2. Specifically, Figures 2(a)–(d) represent stations located at the transitional region (above 40° N), namely Idaho, Boulder, Alpena, and Millstone. These stations generally exhibit stronger and more persistent RSF occurrences. In contrast, Figures 2(e)–(h) illustrate stations located at mid-latitudes (below 40° N), namely Wallops, Melrose, Eglin, and Austin, where the RSF occurrences tend to be weaker and less frequent. This apparent north-south difference further supports the role of latitude in shaping the ionospheric response to geomagnetic and atmospheric disturbances. The enhanced irregularity activity observed in the transitional region may be more strongly influenced by auroral effects and the equatorward penetration of LSTIDs. Paul et al. (2024) observed comparable variations in Spread F occurrences between European stations situated above and below 45°N, suggesting that differing underlying mechanisms drive these irregularities. The authors opined that auroral LSTIDs and MSTIDs emerge as the primary factors contributing to mid-latitude ionospheric irregularity formation.

In contrast to the European sector studied by Paul et al. (2024), which showed that ROTI events over mid-latitude stations such as Juliusruh, Chilton, and Fairford were mostly confined between 18:00 and 05:30 UT and strongly correlated with auroral electrojet activity, the diurnal distribution of ROTI events in the North American dataset shows notable differences.

Specifically, the temporal distribution of ionospheric irregularities does not always align with the European nighttime window, and events are observed to occur both earlier and with less consistency across local time. This discrepancy can be partially attributed to differences in magnetic latitude, longitudinal sector, and the geomagnetic configuration of the North American ionosphere.

3.2 Seasonal Variation

Figures 3 and 4 illustrate the seasonal variation in monthly occurrences of mid-latitude ROTI values exceeding 0.15 TECU/min, specifically during instances of RSF across two distinct latitude bands. In Figure 3, the horizontal axis denotes the months of the year, while the vertical axis indicates the number of days with ROTI enhancements linked to RSF activity. Among the locations analyzed, Idaho shows a notably high occurrence rate of ionospheric irregularities, with a pronounced peak during April (vernal equinoctial period). Additionally, secondary maxima occur in March (vernal equinoctial period) and September (autumnal equinoctial period) shown by Alpena. Similarly, the transitional region stations (Idaho, Boulder, Millstone, and Alpena) experience maximum ionospheric irregularity occurrence, with a secondary peak in March-April as shown in Figure 3(a).

Figure 3(b) illustrates the monthly distribution of ionospheric irregularities observed at mid-latitude digisonde stations within North America. Notably, Austin experienced peak ionospheric irregularity occurrence during November, and Wallops experienced peak ionospheric irregularity occurrence during June-July, particularly in July 2014.

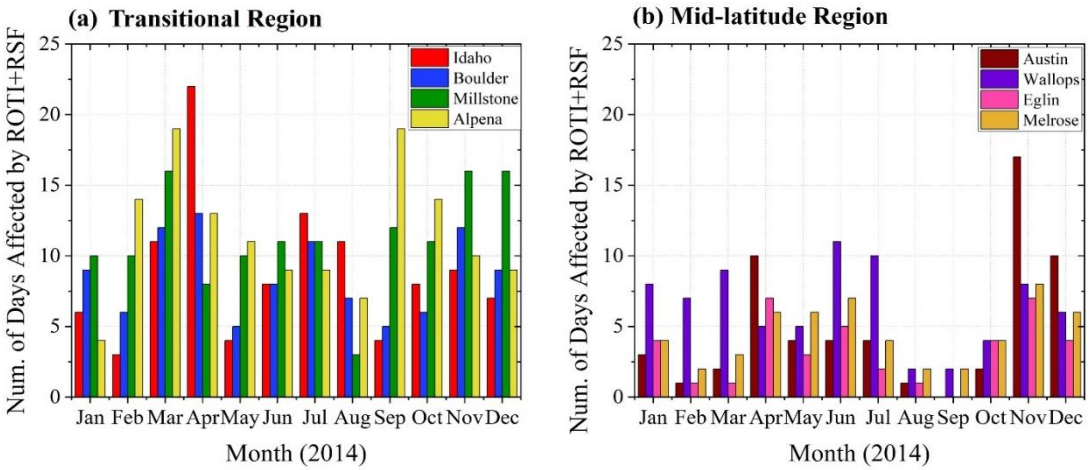

Figure 3: Seasonal patterns in ROTI events associated with RSF were observed across North American transitional and mid-latitude ionospheric regions in 2014, specifically at (a) transitional region digisonde stations such as Idaho, Boulder, Millstone, and Alpena and (b) mid-latitude region digisonde stations including Austin, Wallops, Eglin, and Melrose

Figure 4 presents a comparative analysis of the monthly frequency of ionospheric irregularities observed at transitional and mid-latitude stations. The vertical axis represents the mean number of days impacted by ROTI events linked to recordings from transitional and mid-latitude stations. The transitional stations (indicated by sky colour) predominantly experience irregularities between March and April, while the mid-latitude stations (green colour) are most affected in November.

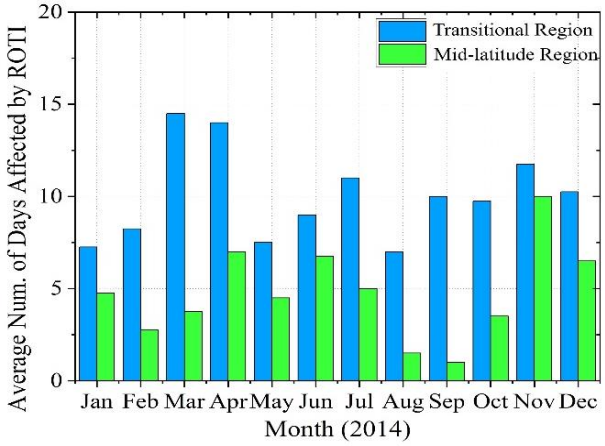

Figure 4: A seasonal comparison of ROTI occurrences linked to RSF was conducted using data from transitional and mid-latitude digisonde stations across North America during 2014

The seasonal variation highlights the latitudinal sensitivity of mid-latitude ionospheric irregularities. The analysis concludes that the transitional stations exhibit peak irregularity occurrences in April, whereas mid-latitude stations peak in November. Findings of the current study are consistent with previous observations by Paul et al. (2023, 2024) that reported similar trends in spread F occurrences across Europe, where upper mid-latitude stations exhibited peaks in winter (December-January) and lower mid-latitude stations in summer (May-August). Liu and Shih-An (2021) also noted that TEC and ROTI activity peaked in late March and May-June, which aligns with the findings of Paul et al. (2023, 2024). Comparing the results of the current study with the previous ones suggests that while seasonal variation in ionospheric irregularities follows a latitudinal pattern, the timing of peaks may differ between North America and Europe, indicating regional variations in ionospheric behaviour.

The analysis reveals that all notable ROTI events exceeding 0.15 TECU/min in 2014 coincided with the presence of RSF and distinct MSTID signatures across the Digisonde stations. These findings indicate that elevated ROTI activity is likely influenced by gravity waves. Furthermore, the diurnal and seasonal behaviours of ROTI occurrences exhibit clear latitude-dependent trends, with maximum activity recorded between 01:30 and 8:30 UT. The peak seasonal occurrence for transitional stations is in April, whereas for mid-latitude digisonde stations, it occurs in November.

3.3 Case Study

3.3.1 Case Study 1: (6 April 2014)

On 6 April 2014, ionospheric irregularities were observed in the transitional region of the North American longitude sector. This period was geomagnetically quiet, with a minimum Dst value of −23 nT. Notably, significant ROTI activity (>0.15 TECU/min) was recorded at all stations during the nighttime on 6 April 2014, as illustrated in Figure 5. Additionally, mid-latitude spread F was detected over the three stations throughout the observation period. At transitional stations in Idaho and Boulder, clear ROTI activity (>0.15 TECU/min) was observed from 06:00 to 14:00 UT. Furthermore, RSF spread F signatures were evident in the ionograms from Idaho and Boulder during this interval. Figure 5 presents a GPS-based ROTI map capturing RSF formation at the corresponding times: Idaho at 08:00 UT, and Boulder at 08:15 UT.

Mrak et al. (2023) highlighted that the concurrent appearance of spread F and ROTI activity indicates the development of large-scale ionospheric irregularities, spanning from a few meters to several tens of kilometers. Similarly, Sivakandan et al. (2020) documented a case of intense ROTI over the mid-latitude ionospheric transition zone in India on 13 June 2018, which aligned with spread F signatures, further confirming the presence of such irregularities.

While multiple investigations have observed the co-occurrence of elevated ROTI values with spread F structures at mid-latitudes, the distinctive feature of this particular case is the sole appearance of RSF. Unlike other spread F types, such as FSF, only RSF was detected alongside significant ROTI enhancements at the Idaho and Boulder stations.

We analyzed detrended TEC (d-TEC) maps during the time interval shown in Figure 6, with Idaho, Boulder, and Alpana marked in pink. Notable d-TEC fluctuations between −0.1 to 0.2 TECU were observed over all two stations from approximately 06:30 to 07:30 UT, indicating the presence of nighttime medium-scale traveling ionospheric disturbances (MSTIDs), as suggested by Haralambous et al. (2023). Similarly, d-TEC maps for Idaho and Boulder revealed comparable fluctuations, reinforcing the occurrence of MSTIDs.

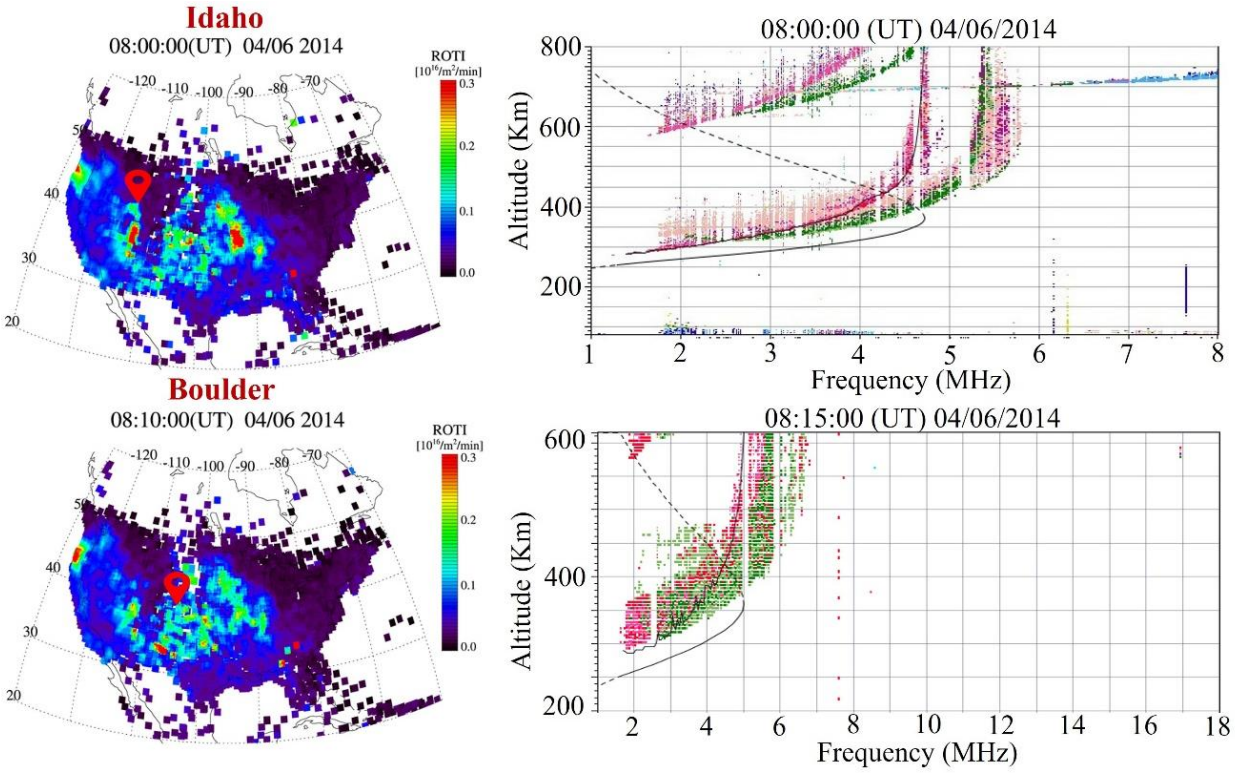

Figure 5: Observation of ROTI occurrences linked to RSF over transitional region digisonde stations Idaho (LT = UT-7h) and Boulder (LT = UT-7h) in the North American longitude sector on 6 April 2014, under geomagnetically quiet conditions (Dst~ −23 nT)

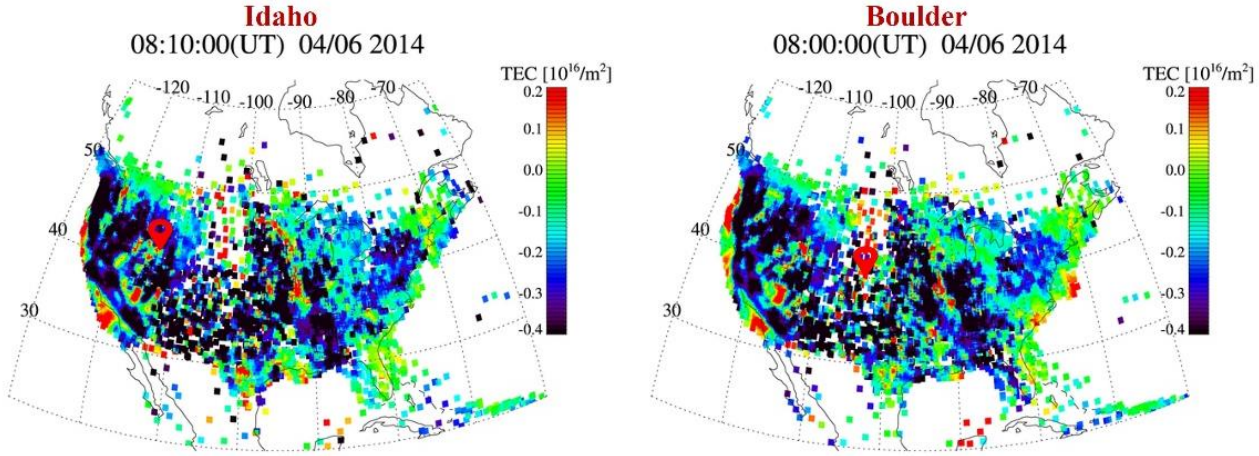

Figure 6: Detrended TEC maps illustrate the positions of the transitional region digisonde stations, Idaho (LT = UT-7h) and Boulder (LT = UT-7h), within the North American longitude sector on April 6, 2014, during a period of relatively quiet geomagnetic conditions (Dst approximately −23 nT)

Previous studies (Paul et al., 2018; Shimazaki et al., 1962) have demonstrated that MSTIDs play a crucial role in the generation of mid-latitude spread F. Additionally, Ye et al. (2023) investigated spread F across Japan at the high-latitude station of Wakkanai (45.4° N, 141.7° E), emphasizing the significance of polarization electric fields in MSTID propagation and spread F formation. Our findings further support the role of gravity wave-induced MSTIDs in the development of RSF, which in turn contributes to enhanced ROTI activity.

3.3.1 Case Study 2: (13 July 2014)

On July 13, 2014, another instance of ionospheric irregularities was recorded under geomagnetically quiet conditions, with a minimum Dst index of −9 nT. Pronounced spread F structures and elevated ROTI values were observed simultaneously at all three transitional digisonde stations, Idaho, Alpana, and Boulder, signaling substantial ionospheric perturbations. Over Idaho, ROTI values exceeding 0.2 to 0.3 TECU/min were recorded from 03:30 to 11:30 UT, along with the presence of RSF. Similarly, between 01:30 and 09:30 UT, significant ROTI activity was noted over Alpana. In Boulder, clear ROTI values in the range of 0.2 to 0.3 TECU/min were observed between 03:30 and 09:30 UT, with RSF also present during this period. Figure 7 provides a visual representation of the concurrent ROTI activity and RSF observed at these locations on 13 July 2014.

From Figure 7, it is evident that strong ROTI activity associated with RSF occurred over Idaho, Alpena, and Boulder around 06:15 UT. Over Alpena, this activity was registered at 03:00 UT, while in Boulder, it was noted around 06:45 UT. Additionally, Figure 8 displays the detrended TEC (d-TEC) maps during this period, highlighting the locations of the three transitional digisonde stations using red markers. MSTID signatures, characterized by d-TEC fluctuations (~−0.4 TECU), were observed at all three stations between 03:00 and 09:00 UT, further confirming the presence of ionospheric disturbances.

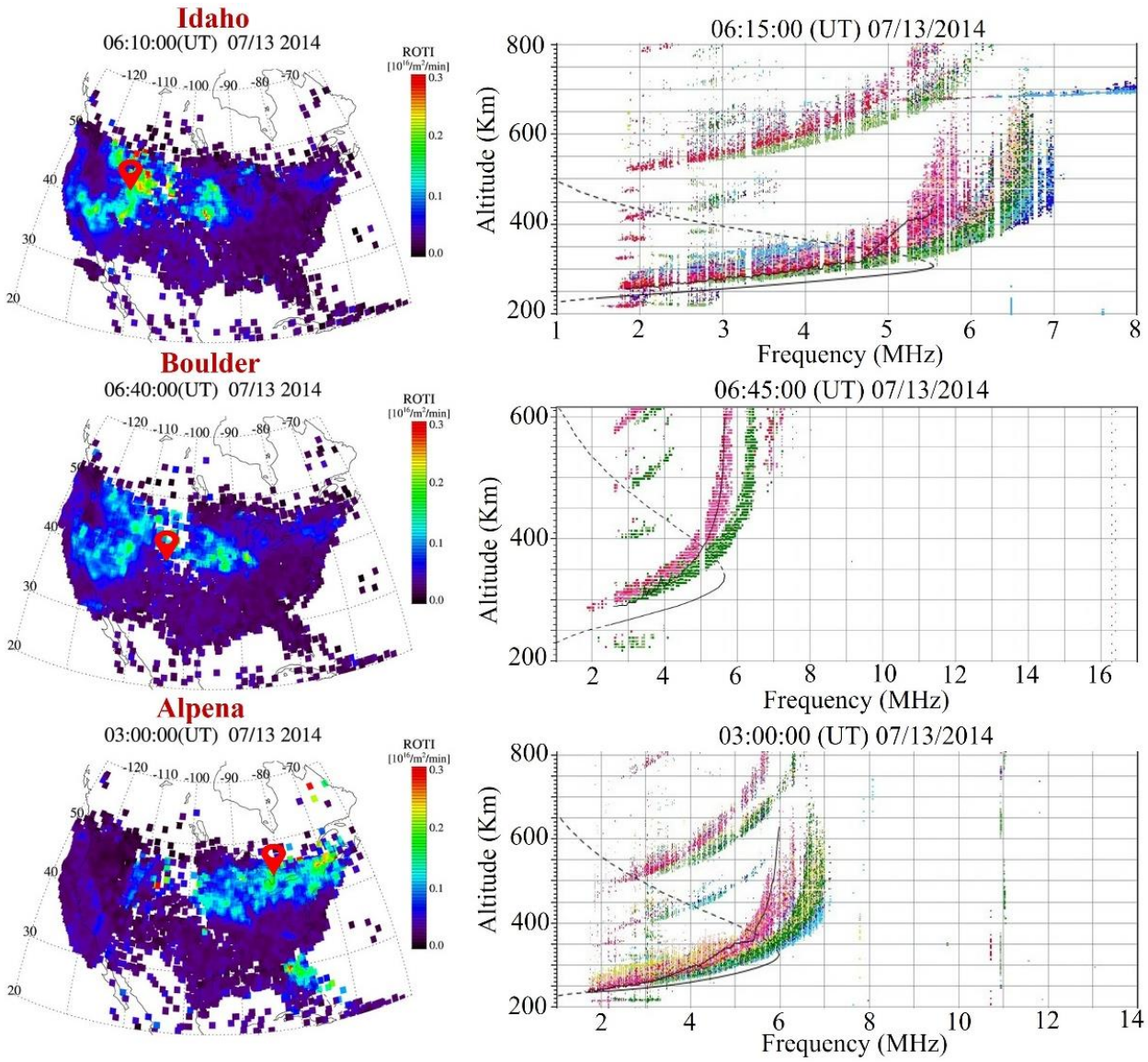

Figure 7: ROTI events associated with RSF were observed on July 13, 2014, at transitional regional digisonde stations, Idaho (LT = UT-7h), Boulder (LT = UT-7h), and Alpena (LT = UT-5h), within the North American longitude sector, during a geomagnetically quiet interval (Dst approximately −9 nT)

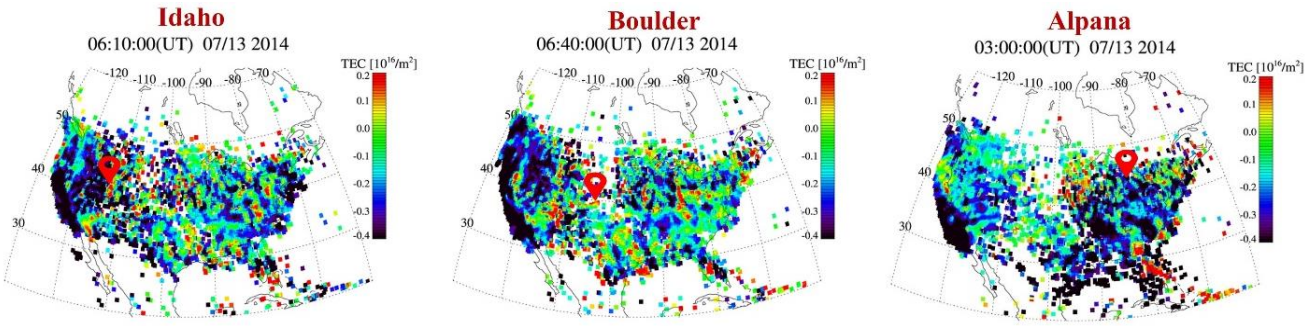

Figure 8: Detrended TEC maps display the positions of the transitional digisonde stations, Idaho (LT = UT-7h), Boulder (LT = UT-7h), and Alpena (LT = UT-5h), within the North American longitude sector on July 13, 2014, during geomagnetically quiet conditions (Dst ~ −9 nT)

The observed ionospheric irregularities, particularly ROTI and RSF, are primarily driven by plasma instabilities in the F-region ionosphere. Spread F, including RSF, occurs due to perturbations in electron density caused by plasma instabilities such as the Perkins instability and gravity wave seeding (Perkins, 1973; Dungey, 1956). These instabilities create large-scale plasma structures that evolve into smaller-scale irregularities, disrupting radio signals and increasing ROTI values. MSTIDs, often linked to atmospheric gravity waves, play a crucial role in generating spread F at mid and high latitudes (Hunsucker, 1982; Paul et al., 2018). Gravity waves, originating from sources like weather systems and auroral activity, induce electric fields that modify plasma dynamics, leading to the development of RSF and associated ionospheric irregularities. The MSTID signatures observed in d-TEC maps further support this connection, demonstrating how wave-driven disturbances contribute to ionospheric structuring and affect signal propagation (Haralambous et al., 2023).

In this case study, the concurrent occurrence of high ROTI and RSF across multiple stations suggests that gravity wave-induced MSTIDs played a key role in triggering plasma irregularities. These findings reinforce the understanding that MSTIDs act as a primary driver of mid-latitude ionospheric disturbances, influencing both the formation of RSF and the enhancement of ROTI activity.

3.3.3 Case Study 3: (5 November 2014)

The impact of the geomagnetic storm in this case study is demonstrated through intense ROTI associated with RSF. This section discusses the spatial and temporal extent of ionospheric irregularities during the storm period. The geomagnetic storm occurred on 5 November 2014, lasting from 00:00 to 19:00 UT, with a minimum Dst value of −43 nT. On this day, ROTI associated with RSF was observed at multiple Digisonde stations across upper and mid-latitudes, as shown in Figure 9.

At transitional region, ROTI (>0.3 TECU/min) was recorded over Idaho from 06:30 UT to 14:00 UT, while Alpena and Millstone Hill experienced high ROTI values (>0.25 TECU/min) between 04:00–14:00 UT. At mid-latitudes shown in Figure 10, Wallops recorded ROTI (>0.3 TECU/min) between 00:00–15:00 UT, while Melrose experienced disturbances from 00:00–17:30 UT. Over Eglin and Austin, high ROTI values (>0.2 TECU/min) were observed from 00:00–19:00 UT. Figures 9 and 10 provide a snapshot of the ionospheric irregularities, showing that geomagnetic disturbances expand the spatial extent of irregularities across both upper and mid-latitudes. A comparison with Figures 5 and 7 further highlights this effect.

Additionally, Figure 11 presents the detrended TEC (d-TEC) maps during this period, marking the locations of the affected Digisonde stations (Idaho, Alpena, Millstone Hill, Wallops, Melrose, Eglin, and Austin) with pink markers. MSTID signatures, characterized by d-TEC fluctuations (~−0.4 TECU), were observed throughout the day at all stations, confirming the presence of ionospheric disturbances.

During geomagnetically quiet periods, as illustrated in Figures 5 and 7, ionospheric irregularities are primarily influenced by neutral atmospheric processes rather than magnetospheric disturbances. MSTIDs, which are often attributed to Perkins instability and atmospheric gravity waves, dominate mid-latitude ionospheric fluctuations (Perkins, 197). These quiet-time irregularities typically exhibit weaker ROTI variations and limited Spread F occurrences, leading to milder impacts on radio signals and GNSS performance (Basu et al., 2002). The absence of strong external forcing means that plasma instabilities evolve more gradually, shaped mainly by thermospheric winds and recombination processes in the F-region.

In contrast, Figures 9 and 10 highlight ionospheric disturbances during geomagnetically active periods, where external drivers such as storm-time electric fields, subauroral polarization streams (SAPS), and enhanced auroral precipitation significantly alter ionospheric dynamics (Huang et al., 2006). During storm events, penetration electric fields can intensify plasma structuring, leading to stronger ROTI values and widespread Spread F occurrences (Abdu, 2012). At high latitudes, Joule heating and particle precipitation enhance conductivity, triggering global-scale circulation changes through the disturbance dynamo effect (Blanc & Richmond, 1980). The comparison of Figures 5, 7, 9, and 10 underscores the fundamental differences in the formation of ionospheric irregularities under quiet and disturbed conditions, emphasizing the role of magnetospheric inputs in amplifying plasma turbulence and affecting GNSS reliability.

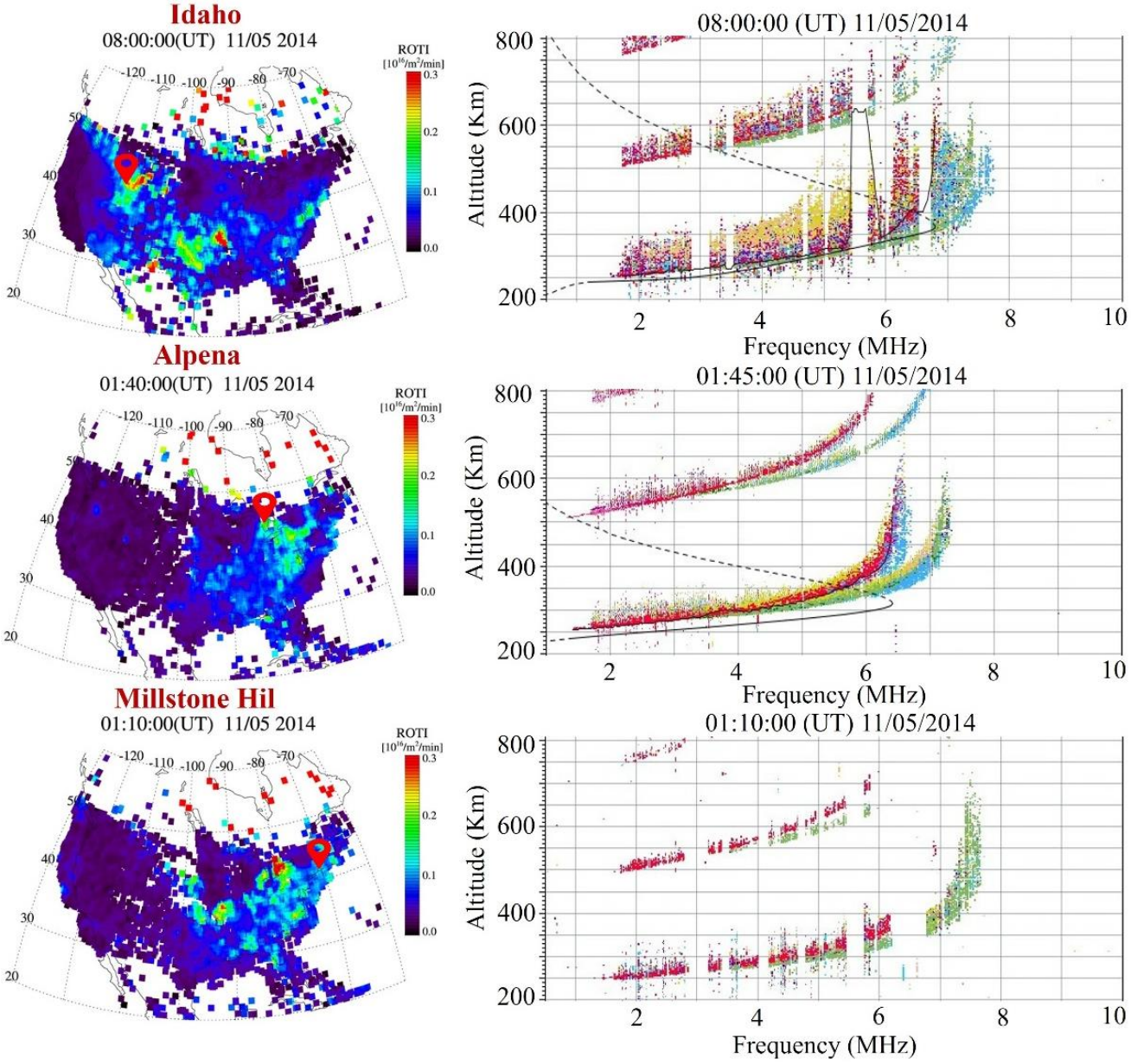

Figure 9: Examination of ROTI events associated with RSF across three transitional region digisonde station Idaho (LT = UT-7h), Alpena (LT = UT-5h), and Millstone Hill (LT = UT-8h), in the North American region, specifically on November 5, 2014, during geomagnetic disturbances (Dst ~ −43 nT)

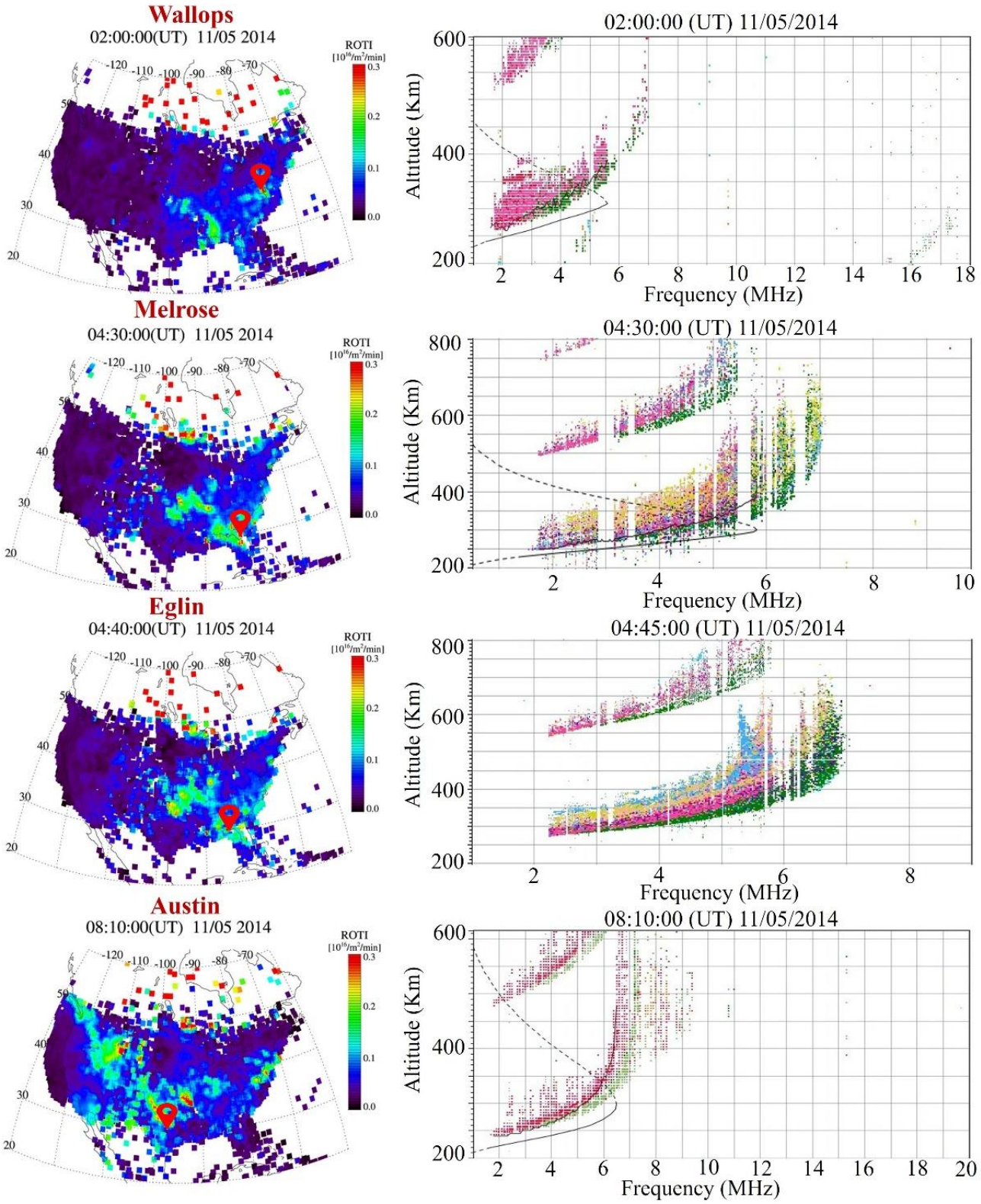

Figure 10: Examination of ROTI events associated with RSF across four mid-latitude digisonde stations Wallops (LT = UT-5h), Melrose (LT = UT-5h), Eglin (LT = UT-5h), and Austin (LT = UT-6h), in the North American region, specifically on November 5, 2014, during geomagnetic disturbances (Dst ~ −43 nT)

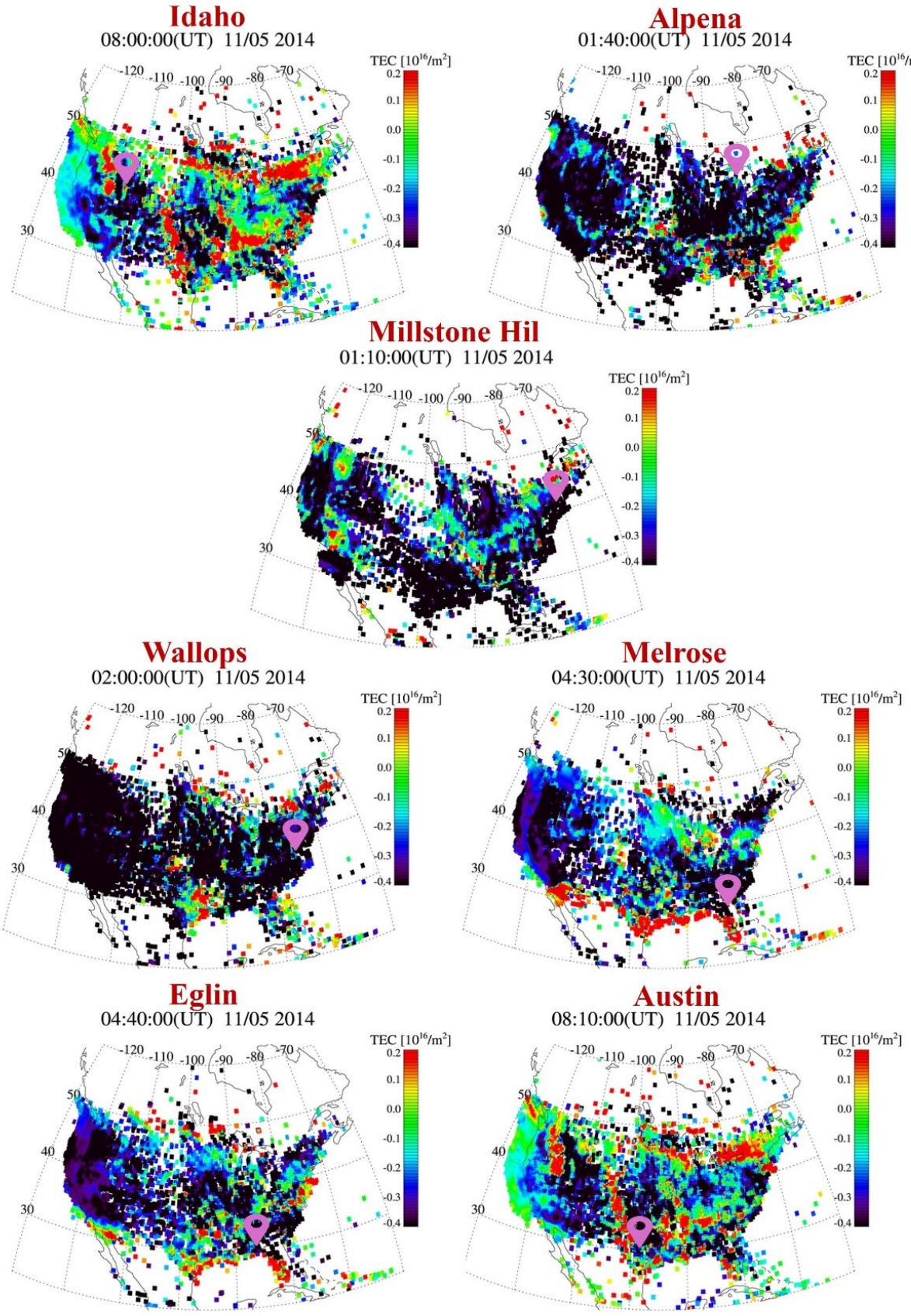

Figure 11: Detrended TEC maps showing the locations of three transitional digisonde stations Idaho (LT = UT-7h), Alpena (LT = UT-5h), and Millstone Hill (LT = UT-5h) and four Mid-latitude Digisonde stations (Wallops (LT = UT-5h), Melrose (LT = UT-5h), Eglin (LT = UT-5h), and Austin (LT = UT-6h) in the North American longitude sector on 5 November 2014, under geomagnetically disturbed conditions (Dst ~ −43 nT)

3.3.4 Case Study 4: (19 February 2014)

An intriguing case of ROTI activity is illustrated in Figure 12, depicting the evolution of spread F over Idaho from 07:00 UT to 11:00 UT on 19 February 2014 under geomagnetically disturbed conditions, with a minimum Dst index of −98 nT. In our study, spanning 97 days, we examined approximately 17,280 spread F events over eight stations, among which only two events (0.008%) were identified as possible FSF. In a previous study, Paul et al., (2024) observed spread F occurrences 53 days in a year but detected one FSF event. These observations reinforce the predominance of RSF and the negligible occurrence of FSF in our dataset. Therefore, we excluded FSF from the correlation analysis, focusing instead on the more frequent and geophysically impactful RSF events.

A comparable progression is evident in Figure 12: RSF is initially observed at 07:00 UT, followed by increasing range ambiguity between 08:00 UT and 09:50 UT, which developed into a mixed spread F (MSF) structure and ultimately evolved into FSF after 10:00 UT. During this period, high ROTI values ranging from approximately 0.2 to 0.25 TECU/min were recorded, coinciding with the RSF activity. After 11:00 UT, ROTI decreased to about 0.1 TECU/min, corresponding with the MSF phase, and dropped further to 0.05 TECU/min during the FSF development around 04:00 UT. As noted by Paul et al. (2018), the RSF to FSF transition involves the gradual dissipation of plasma instabilities at increasing F-layer altitudes, leading to the formation of FSF during post-midnight hours. This sequence is consistent with the interpretation by King (1970), who proposed that FSF represents the decay product of RSF.

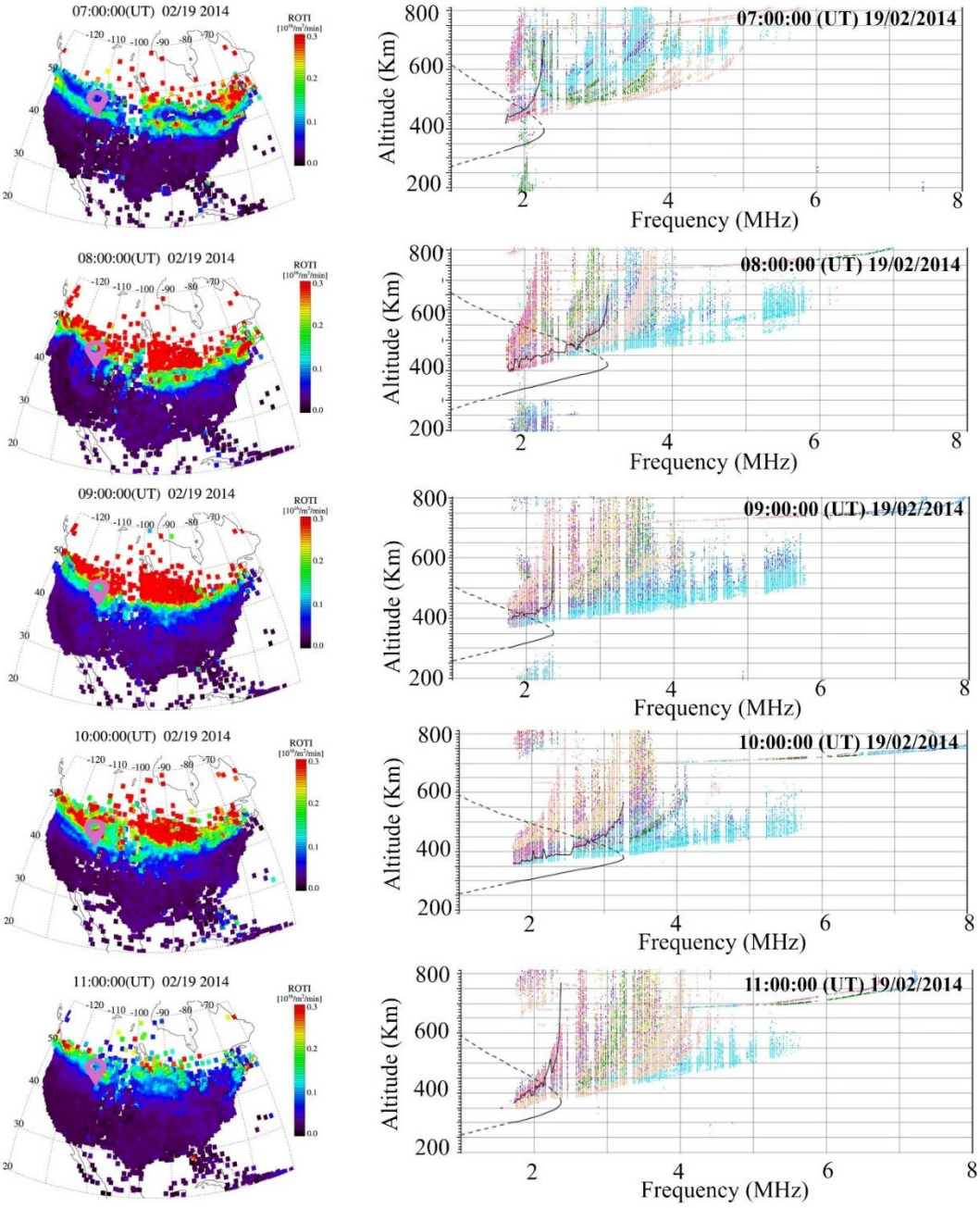

Figure 12: A case study of ROTI activity during RSF to FSF evolution over Idaho (LT = UT-7h), recorded on 19 February 2014 during geomagnetically disturbed conditions (Dst~- 98 nT)

Figure 13 presents the d-TEC maps of the Idaho stations during the evolution from RSF to FSF. The station locations in Idaho are indicated by pink markers. Clear MSTID signatures were observed in the d-TEC data, with values reaching approximately −0.4 TECU, during the period from 07:00 to 11:00 UT on 19 February 2014. These disturbances typically arise during geomagnetic storms, where Joule heating and particle precipitation from the magnetosphere are the main drivers of this effect (King et al., 1970). Joule heating increases the temperature of the upper thermosphere at mid-latitudes, intensifying high-speed neutral winds through ion drag. As a result, gravity waves and wind surges propagate from high latitudes toward the equatorial region via the mid-latitude ionosphere. MSTIDs are a visible outcome of this dynamic process, also illustrated in Figure 13.

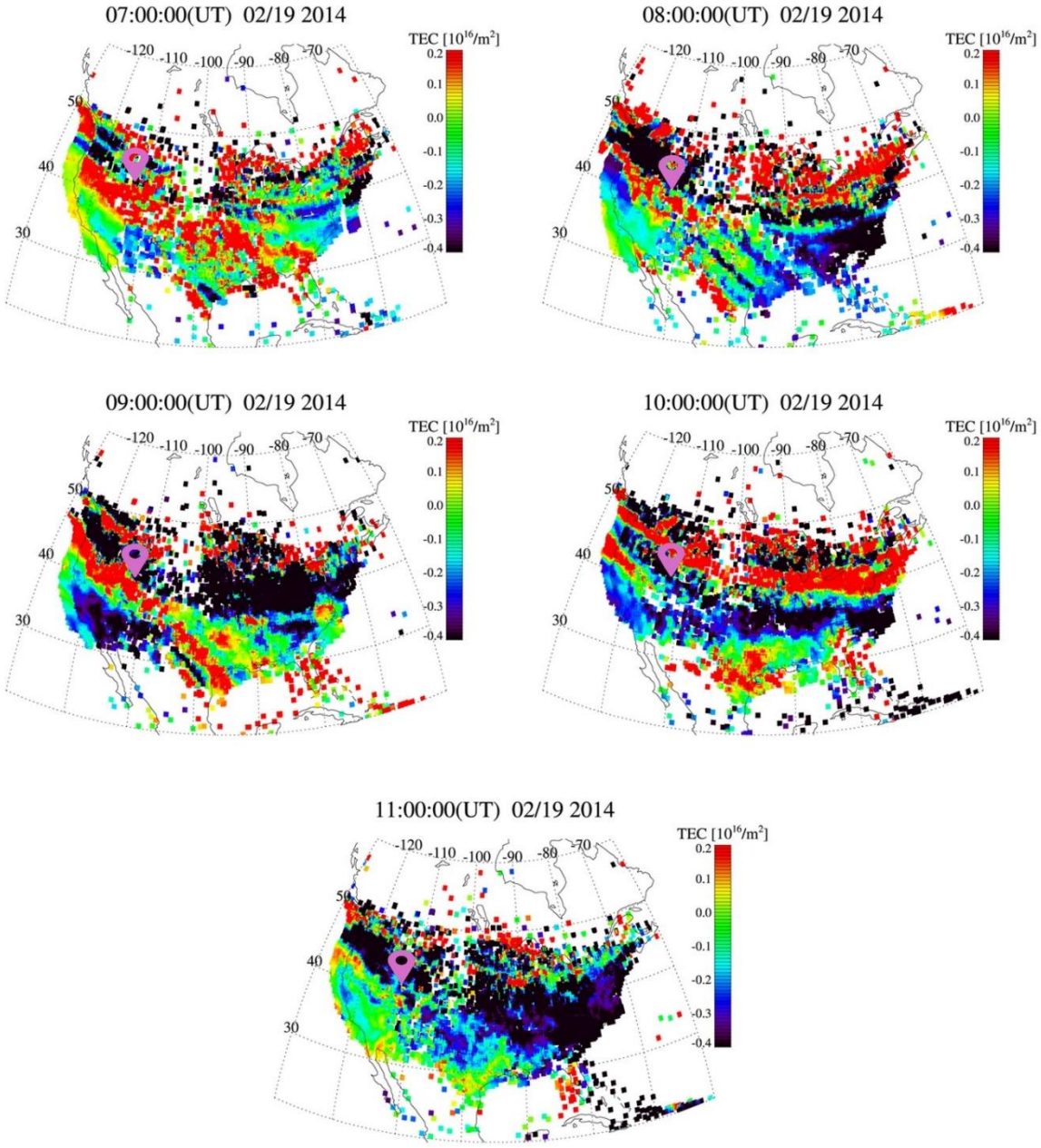

Figure 13: Detrended TEC maps with locations of Idaho (LT = UT-7h), recorded on 19 February 2014 during geomagnetically disturbed conditions (Dst~- 98 nT)

Table 2 presents a comparison between the present study and two recent studies by Paul et al. (2024) and Hong et al. (2024), focusing on ionospheric irregularities across different geographical regions, time periods, and solar cycle phases.

Paul et al. (2024) investigated the correlation between the ROTI and Spread-F occurrences during a low-to-moderate solar activity year (2011) in Solar Cycle 24. Their analysis categorized 271 days as geomagnetically quiet (Dst > -25 nT) and 94 days as disturbed (Dst < -25 nT) out of the 365 days. Notably, ROTI values exceeded 0.15 TECU/min on 97 days, with Spread-F events coinciding on 53 of these days.

The present study examines the relationship between the ROTI and Spread-F phenomena during 2014, a year of intensified solar activity within Solar Cycle 24. Analysis

revealed that 132 days were classified as geomagnetically disturbed during this period. ROTI values exceeded 0.15 TECU/min on 247 days, with Spread-F events coinciding on 92 of these days, as shown in Table 2.

These results underscore the significant impact of elevated solar activity on ionospheric irregularities. The increased prevalence of geomagnetically disturbed days, coupled with the higher frequency of ROTI enhancements and Spread-F events, highlights the critical role of solar-driven processes in modulating ionospheric dynamics during periods of intense solar activity.

During solar maxima, solar flux intensifies ionospheric instability, driving frequent and intense equatorial plasma bubbles (EPBs) and electron densities (Abdu, 2012; Carter et al., 2014). These conditions foster the development of pronounced RSF and enhanced GNSS phase scintillations, which in turn elevate ROTI values (Zakharenkova et al., 2020).

In contrast, low solar activity periods (e.g., solar minima) exhibit reduced solar extreme ultraviolet (EUV) flux, weaker ionospheric plasma density gradients, and diminished EPB occurrence rates (Aa et al., 2020). The subdued F-region vertical drifts and weaker equatorial electrojet currents during these periods lead to less frequent RSF and milder scintillations, resulting in lower ROTI values. The marked differences in both the frequency of ROTI events and Spread-F detection highlight the significant impact of solar activity levels on ionospheric irregularity occurrence and intensity.

Ionospheric irregularities are strongly influenced by latitude, as the ionospheric density and structure vary with geomagnetic and geographic latitudes (Kelley, 2009). The presence of the equatorial ionization anomaly (EIA) affects ionospheric irregularities differently in equatorial, low-latitude, and mid-latitude regions (Aarons et al., 1980). For instance, studies in Europe (Paul et al., 2024) and North America (Present Study) typically observe irregularities at higher latitudes, where the effects of MSTIDs are more pronounced. In contrast, studies in equatorial and low-latitude regions, such as those by Hong et al. (2024), focus more on the dynamics of ESF and plasma bubbles, which are dominant in these regions due to different geomagnetic and atmospheric conditions.

Seasonal variation in ionospheric irregularities is influenced by the annual cycle of solar insolation, which affects the ionization rates in the ionosphere, as well as the position of the geomagnetic equator relative to the Sun (Blanc and Richmond, 1980). In regions like Europe, irregularities tend to peak in winter (Paul et al., 2024), while in North America, as observed in the present study, the peak is during the transition months of March, April, and November, likely due to the different solar zenith angles and atmospheric conditions during these seasons. The variation in solar activity also influences the intensity and occurrence of irregularities, as higher solar flux results in increased ionization and enhanced dynamics in the ionosphere, particularly during the high solar activity period (Basu et al., 2001). During different solar cycle phases, the intensity and distribution of ionospheric irregularities may vary significantly, with enhanced irregularities typically observed during solar maximum, as seen in the Present Study (2014, solar cycle 24 maximum).

Table 2: Comparison of the Present Study with Previous Case Studies on Ionospheric Irregularities

Criteria	Paul et al. (2024)	Hong et al. (2024)	Present Study (2025)
Location	Europe (35°N-70°N, -10°E-40°E)	Asia (0°N-25°N, 95°E-115°E)	North America (15°N-50°N, 70°W-125°W)
Period	2011	2023	2014
Solar Cycle	Ascending phase of solar cycle 24	Ascending phase of solar cycle 25	High solar cycle 24
Geomagnetically Quite days	271 days	253 days	233 days
Geomagnetically Disturbed days	94 days	112 days	132 days
ROTI > 0.15 TECU/min	97 days	Not Mentioned	247 days
Spread F Occur	53 days	Not mentioned	92 days
Number of Stations	8	2	8
Diurnal Variation of ROTI	Maximum irregularities at night (18:00–05:00 UT)	Maximum irregularities at night (19:15–23:15 UT)	Maximum irregularities at night (01:30–08:30 UT)
Seasonal Variation	January and July	March, April, and October	March, April, and November
ROTI Driving Mechanisms	Equatorial spread F, Gravity waves, and MSTID	Equatorial spread F, plasma bubbles, and MSTID	Equatorial spread F, Gravity waves, MSTIDs, and polarization electric fields

At night, ionospheric instabilities and irregularities typically increase due to the cessation of solar ionization, which allows the recombination of ions and the formation of instability layers (Perkins, 1973). The exact timing of peak irregularities can vary across studies depending on the local ionospheric conditions and the region's geomagnetic characteristics. For example, studies in the mid-latitude regions (Present Study) observe maximum irregularities during the early nighttime hours (01:30–08:30 UT), whereas studies in other regions report peaks at different local times, such as Hong et al. (2024), which observed maxima from 19:15 to 23:15 UT. These differences can be attributed to variations in the local time of sunset, the altitude of the ionospheric F-layer, and the local thermospheric conditions.

Furthermore, polarization electric fields play a significant role in the generation of ionospheric irregularities at higher latitudes, particularly during high solar activity, when increased ionization leads to enhanced electric fields that destabilize the ionosphere (Huang et al., 2012). The observed dissimilarities in ionospheric irregularities across different studies can be attributed to the combined effects of latitude-dependent ionospheric dynamics, local thermospheric conditions, solar activity, and geographic factors. These factors interact to produce region-specific irregularity characteristics, highlighting the importance of considering the spatial and temporal context when studying ionospheric irregularities.

Although the paper discusses a potential correlation between ROTI and Spread F (particularly RSF), statistical correlation analysis was not conducted due to key limitations in the dataset. Specifically, both ROTI and ionogram data were classified into binary categories (Present/Absent), limiting the statistical resolution. Furthermore, a mismatch in temporal resolution exists, ROTI maps are generated at 10-minute intervals, while ionogram sampling intervals vary across stations (see Table 1). Additionally, RSF events often persist across multiple ionograms, complicating the temporal alignment between ROTI fluctuations and RSF occurrences. These factors collectively rendered conventional statistical methods unsuitable for robust correlation analysis.

4. CONCLUSION

This study provides a comprehensive investigation of mid-latitude ionospheric irregularities over North America by integrating Digisonde ionograms, high-resolution ROTI and d-TEC maps, and geomagnetic indices. Our results reveal that the seasonal and latitudinal variations of Spread F occurrences and ROTI fluctuations are strongly linked to MSTIDs and geomagnetic activity. A clear seasonal dependence was observed, with upper and mid-latitude stations peaking in April and lower mid-latitude stations exhibiting maximum irregularity occurrences in November.

Through detailed case studies, we demonstrated that MSTIDs, likely driven by gravity wave dynamics, play a crucial role in generating plasma irregularities, which in turn enhance ROTI values and contribute to Spread F formation. Under quiet geomagnetic conditions, these irregularities exhibit a strong nighttime preference. Conversely, during disturbed geomagnetic conditions, as seen in the November 5, 2014, geomagnetic storm, the spatial extent of ionospheric irregularities increased significantly, affecting both upper and lower mid-latitude stations for both daytime and nighttime.

These findings offer new insights into the mechanisms governing mid-latitude ionospheric disturbances, reinforcing the role of MSTIDs in the formation of Spread F and ROTI enhancements. Our study highlights the necessity of continuous, high-resolution monitoring of ionospheric irregularities to improve space weather forecasting and mitigate the impact of ionospheric disturbances on GNSS-based navigation and communication systems.

This study focused solely on the detection of Spread F presence or absence, not on subtype classification. Therefore, the risk of interpretive variation was limited. We acknowledge that automated classification techniques, including machine learning approaches, hold promise for large-scale, objective subtype analysis. However, these methods were not within the scope of the present work and are suggested as a potential direction for future research.

To operationalize ROTI–Spread F correlations in real-time space weather forecasting, the following strategies are proposed:

a) Dynamic ROTI Threshold Alerts: Implement adaptive ROTI thresholds (e.g., >0.15 TECU/min) to flag potential RSF events, enabling timely warnings for GNSS users about probable ionospheric irregularities.

b) Model Assimilation: Integrate real-time ROTI data into advanced ionospheric forecast systems such as Global Assimilation of Ionospheric Measurements (GAIM) and Thermosphere-Ionosphere-Electrodynamics General Circulation Model (TIE-GCM) to improve the accuracy and responsiveness of space weather forecasts.

c) Multi-Instrument Fusion: Combine ROTI data with complementary ionosonde measurements and optical observations (e.g., airglow imaging) to create a comprehensive, multi-dimensional situational awareness of ionospheric conditions.

d) Machine Learning Optimization: Employ machine learning models trained on ROTI time-series alongside geophysical indices (such as Kp, Dst, and solar flux) to enhance predictive estimates of Spread F occurrence and intensity.

e) GNSS Resilience Enhancements: Incorporate ROTI-based quality flags into GNSS receiver algorithms to identify and exclude compromised signals during high-disturbance periods, thereby mitigating positioning errors and improving system robustness.

f) Automated Spread F Subtype Classification: Develop and apply automated classification models to distinguish between Spread F subtypes. Future research could explore methods such as convolutional neural networks (CNNs), support vector machines (SVMs), or decision tree classifiers trained on labeled ionogram datasets to enable large-scale, objective subtype analysis

These measures collectively advance the precision of ionospheric disturbance forecasts, bolstering the reliability of GNSS navigation and communication systems during space weather events.

ACKNOWLEDGMENTS

We are grateful to Kyoto University, Japan (https://wdc.kugi.kyoto-u.ac.jp/dst_final/, accessed on 02 March 2025) for providing the geomagnetic data and Digital Ionograms database (DIDBase) of the Global Ionospheric Radio Observatory (GIRO) portal (http://giro.uml.edu, accessed on 02 March 2025) for the ionograms of 2014. We acknowledge the use of ROTI and detrended GPS TEC maps over North America for 2014, which are available at https://aer-nc-web.nict.go.jp/GPS/N_AMRC/, accessed on 02 March 2025.

AUTHOR DECLARATION

The authors declare no conflicts of interest.

DATA AVAILABILITY STATEMENT

In this study, we utilized TEC maps, both ROTI and detrended TEC, over North America, which were obtained from the (https://aer-nc-web.nict.go.jp/GPS/N_AMRC/, accessed on 10 January 2025). Additionally, ionogram data for the year 2014 from stations located in Idaho, Boulder, Alpena, Millstone Hill, Wallops, Melrose, Eglin, and Austin were accessed from the DIDBase at https://lgdc.uml.edu/common/DIDBFastStationList (accessed on 10 January 2025). All data sources are publicly accessible and free of charge.

FUNDING INFORMATION

This research received no external funding.

REFERENCES

Aarons, J., Basu, S. and Bushby, S.J., 1980. Latitudinal and seasonal variation of F-layer irregularities. Radio Science, 15(3), pp. 401-404.

Aarons, J., 1993. The role of the ring current in the generation or inhibition of equatorial F layer irregularities during magnetic storms. Radio Science, 28(4), pp. 469-475.

Aa, E., Huang, W., Yu, S., Liu, S., Li, J., & Zhang, S. (2020). Statistical analysis of ionospheric irregularities and scintillation during solar minimum. Journal of Geophysical Research: Space Physics, 125(8), https://doi.org/10.1029/2020JA028123.

Abdu, M.A., 2012. Equatorial spread F/plasma bubble irregularities under storm time disturbance electric fields. Journal of atmospheric and solar-terrestrial physics, 75, pp.44-56.

Alfonsi, L., De Franceschi, G., Spogli, L. and Tommaso, G.D., 2013. Ionospheric scintillations over Europe at different solar activity conditions. Journal of Space Weather and Space Climate, 3(A06).

Basu, S. and Kelley, M.C., 1979. A review of recent observations of equatorial scintillations and their relationship to current theories. Radio Science, 14(3), pp. 471-485.

Basu, S., Groves, K.M., Quinn, J.M., & Doherty, P. (1999). A comparison of TEC fluctuations and scintillations at Ascension Island. *Journal of Atmospheric and Solar-Terrestrial Physics, 61*(16), 1219–1226.

Basu, S., Groves, K.M., Quinn, J.M. and Doherty, P., 2001. A comparison of TEC fluctuations and scintillations at Ascension Island. Journal of Atmospheric and Solar-Terrestrial Physics, 63(9), pp. 959-964.

Basu, S., Basu, S., Groves, K.M., Weber, E.J., Sultan, P.J. and Keskinen, M.J., 2002. Characteristics of plasma structuring in the mid-latitude and equatorial ionosphere during severe magnetic storms. Journal of Geophysical Research: Space Physics, 107(A12), pp. 1-14.

Basu, S., Kudeki, E., Basu, S., Valladares, C.E., Weber, E.J., Zengingonul, H.P., Bhattacharyya, S., Sheehan, R., Meriwether, J.W., Biondi, M.A. and Kuenzler, H., 1996. Scintillations, plasma drifts, and neutral winds in the equatorial ionosphere after sunset. Journal of Geophysical Research: Space Physics, 101(A12), pp.26795-26809.

Berkner, L.V., & Wells, H.W. (1934). F-region ionosphere investigations at low latitudes. *Terrestrial Magnetism and Atmospheric Electricity, 39*(3), 215–230.

Blanc, M. and Richmond, A.D., 1980. The ionospheric disturbance dynamo. Journal of Geophysical Research: Space Physics, 85(A4), pp.1669-1686.

Bowman, G.G.; Monro, P.E. Mid-latitude range spread and travelling ionospheric disturbances. J. Atmos. Terr. Phys. 1988, 50, 215–223.

Bowman, G.G. (1991). Ionospheric frequency spread and its relationship with range spread in mid-latitude regions. *Journal of Geophysical Research: Space Physics, 96*(6), 9745–9753.

Bowman, G.G. (1998). Short-term delays (hours) of ionospheric spread F occurrence at a range of latitudes, following geomagnetic activity. *Journal of Geophysical Research: Space Physics, 103*(A5), 11627–11634.

Burke, W. J., Gentile, L. C., Huang, C. Y., Valladares, C. E., & Su, S.-Y. (2004). Longitudinal variability of equatorial plasma bubbles observed by DMSP and ROCSAT-1. Journal of Geophysical Research: Space Physics, 109(A12), A12301. https://doi.org/10.1029/2004JA010583.

Carter, B. A., Yizengaw, E., Pradipta, R., Retterer, J. M., Groves, K., Valladares, C., ... & Roddy, P. (2014). Global equatorial plasma bubble occurrence during the 2015 St. Patrick's Day storm. Journal of Geophysical Research: Space Physics, 121(1), 894–905. https://doi.org/10.1002/2015JA022194.

Chandra, H., Rastogi, R.G. and Sastri, J.H., 2003. Equatorial Spread F and its latitudinal variations. Annales Geophysicae, 21(4), pp. 899-907.

Cherniak, I., Krankowski, A. and Zakharenkova, I., 2014. Observation of the ionospheric irregularities over Europe. Journal of Geophysical Research: Space Physics, 119(8), pp. 6773-6786.

Cherniak, I., Zakharenkova, I., & Krankowski, A. (2014). Approaches for modelling ionospheric irregularities based on the TEC rate index. *Earth, Planets and Space, 66*(1), 165.

Cherniak, I., Krankowski, A., & Zakharenkova, I. (2018). ROTI Maps: A new IGS ionospheric product characterizing the ionospheric irregularities occurrence. *GPS Solutions, 22*(2), 69.

Cherniak, I., Zakharenkova, I. and Redmon, R.J., 2018. Dynamics and occurrence of GPS scintillations over the high latitudes. Space Weather, 16(10), pp. 1345-1359.

Cherniak, I.; Zakharenkova, I.; Krankowski, A. IGS ROTI maps: Current status and its extension towards equatorial region and southern hemisphere. Sensors 2022, 22, 3748.

Chatterjee, D., Pathan, R. and Pallamraju, D., 2020. Response of equatorial plasma bubbles to geomagnetic storms using GNSS ROTI and ground-based airglow observations. Advances in Space Research, 66(12), pp. 2809-2822.

Das Gupta, A., Basu, S., Basu, S. and Das, S.K., 1981. Equatorial scintillations: Relationship to the development of irregularities in the post-sunset ionosphere. Journal of Atmospheric and Terrestrial Physics, 43(8), pp. 815-823.

Dabas, R.S., Reddy, B.M. and Das Gupta, A., 2003. Equatorial ionospheric irregularities and their effects on trans ionospheric propagation. Advances in Space Research, 31(3), pp. 509-518.

Dabas, R.S., Das, R.M., Sharma, K., Chopra, P. and Gwal, A.K., 2007. Ionospheric irregularities and GPS positioning errors. Advances in Space Research, 39(10), pp. 1514-1520.

Davies, K., 1990. Ionospheric radio (No. 31). Peter Peregrinus Ltd., London.

Dungey, J.W., 1956. Convective diffusion in the equatorial F region. Journal of Atmospheric and Terrestrial Physics, 9(5-6), pp.304-310.

Hunsucker, R.D., 1982. Atmospheric gravity waves generated in the high-latitude ionosphere: A review. Reviews of Geophysics, 20(2), pp.293-315.

Huang, C.S., de La Beaujardiere, O., Roddy, P.A., Hunton, D.M., Liu, J.Y., Chen, K. and Hei, M., 2012. Statistical analysis of the zonal drift velocity of equatorial plasma bubbles observed by the C/NOFS satellite. Journal of Geophysical Research: Space Physics, 117(A5), A05317.

Huang, C.S.; Miller, C.A.; Kelley, M.C. Basic properties and gravity wave initiation of the mid-latitude F region instability. Radio Sci. 1994, 29, 395–405.

Huang, C.S, Sazykin, I., Spiro, R., Goldstein, J., Crowley, G. and Ruohoniemi, J.M., 2006. Storm-time penetration electric fields and their effects.

Kelley, M.C., 2009. The Earth's Ionosphere: Plasma Physics and Electrodynamics. Elsevier.

Kotulak, K., Zakharenkova, I., Krankowski, A., Cherniak, I., Wang, N., & Fron, A. (2020). Climatology characteristics of ionospheric irregularities described with GNSS ROTI. *Remote Sensing*, *12*(16), 2634.

Kintner, P.M., Jr., Coster, A.J., Fuller-Rowell, T., Mannucci, A.J., Mendillo, M., & Heelis, R. (Eds.). (2013). *Mid-latitude Ionospheric Dynamics and Disturbances*. John Wiley & Sons: Hoboken, NJ, USA. Volume 181.

King, G.A.M., 1970. Spread-F on ionograms. Journal of Atmospheric and Terrestrial Physics, 32(2), pp.209-221.

Maruyama, T., & Matuura, N. (1984). Longitudinal variability of annual changes in activity of equatorial spread F and plasma bubbles. Journal of Geophysical Research: Space Physics, 89(A12), 10903–10912.

Miller, C.A.; Swartz, W.E.; Kelley, M.C.; Mendillo, M.; Nottingham, D.; Scali, J.; Reinisch, B. Electrodynamics of mid-latitude spread F: 1. Observations of unstable, gravity wave-induced ionospheric electric fields at tropical latitudes. J. Geophys. Res. Space Phys. 1997, 102, 11521–11532.

Monte-Moreno, E., Hernandez-Pajares, M., Yang, H., Rigo, A.G., Jin, Y., Høeg, P., Miloch, W.J., Wielgosz, P., Jarmołowski, W., Paziewski, J. and Milanowska, B., 2021. Method for forecasting ionospheric electron content fluctuations based on the optical flow algorithm. IEEE Transactions on Geoscience and Remote Sensing, 60, pp.1-21., doi: 10.1109/TGRS.2021.3126888.

Mrak, S.; Coster, A.; Groves, K.; Nikoukar, R. Ground-based infrastructure for observing and characterizing GNSS scintillation producing ionospheric irregularities at mid-latitudes. Bull. Am. Astron. Soc. 2023, 55, 286.

Narayanan, V.L.; Shiokawa, K.; Otsuka, Y.; Neudegg, D. On the role of thermospheric winds and sporadic E layers in the formation and evolution of electrified MSTIDs in geomagnetic conjugate regions. J. Geophys. Res. Space Phys. 2018, 123, 6957–6980.

Nguyen, C.T., Oluwadare, S.T., Le, N.T., Alizadeh, M., Wickert, J. and Schuh, H., 2021. Spatial and temporal distributions of ionospheric irregularities derived from regional and global ROTI maps. Remote Sensing, 14(1), p.10, doi: 10.3390/rs14010010.

Otsuka, Y.; Shiokawa, K.; Ogawa, T.; Yokoyama, T.; Yamamoto, M. Spatial relationship of nighttime medium-scale travelling ionospheric disturbances and F region field-aligned irregularities observed with two spaced all-sky airglow imagers and the middle and upper atmosphere radar. J. Geophys. Res. Space Phys. 2009, 114.

Otsuka, Y.; Onoma, F.; Shiokawa, K.; Ogawa, T.; Yamamoto, M.; Fukao, S. Simultaneous observations of nighttime medium-scale travelling ionospheric disturbances and E region field-aligned irregularities at mid-latitude. J. Geophys. Res. Space Phys. 2007, 112.

Otsuka, Y.; Suzuki, K.; Nakagawa, S.; Nishioka, M.; Shiokawa, K.; Tsugawa, A. GPS observations of medium-scale traveling ionospheric disturbances over Europe. Ann. Geophys. 2013, 31, 163–172.

Paul, K.S.; Haralambous, H.; Oikonomou, C.; Paul, A. Investigation of Satellite Trace (ST) and Multi-reflected Echo (MRE) ionogram signatures and its possible correlation to nighttime spread F development from Cyprus over the solar mini-max (2009–2016). Adv. Space Res. 2021, 67, 1958–1967.

Paul, K.S.; Haralambous, H.; Oikonomou, C.; Paul, A.; Belehaki, A.; Ioanna, T.; Kouba, D.; Buresova, D. Multi-station investigation of spread F over Europe during low to high solar activity. J. Space Weather Space Clim. 2018, 8, A27.

Paul, K.S.; Haralambous, H.; Oikonomou, C.; Paul, A. Long-term aspects of nighttime spread F over a low mid-latitude European station. Adv. Space Res. 2019, 64, 1199–1216.

Paul, K.S.; Haralambous, H.; Singh, A.K.; Gulyaeva, T.L.; Panchenko, V.A. Mid-latitude Spread F, long-term occurrence characteristics as a function of latitude over Europe. Adv. Space Res. 2022, 70, 710–722.

Paul, K.S.; Haralambous, H.; Oikonomou, C.; Singh, A.K.; Gulyaeva, T.L.; Panchenko, V.A.; Altadill, D.; Buresova, D.; Mielich, J.; Verhulst, T. A mid-latitude spread F over an extended European area. J. Atmos. Sol.-Terr. Phys. 2023, 248, 106093.

Paul, K.S., Rafi, M.H., Haralambous, H. and Mostafa, M.G., 2024. Assessing ionospheric irregularity differences over Europe using ROTI and ionosonde data. Atmosphere, 15(1), p.120001.

Perna, L., Belehaki, A. and Zolesi, B., 2018. Ionospheric irregularities over Europe as derived from GNSS data. Annales Geophysicae, 36(5), pp. 1243-1254.

Perkins, F., 1973. Ionospheric irregularities. Reviews of Geophysics, 11(4), pp. 779-822.

Pi, X., Mannucci, A.J., Lindqwister, U.J., & Ho, C.M. (1997). Monitoring of global ionospheric irregularities using the worldwide GPS network. *Geophysical Research Letters, 24*(19), 2283–2286.

Reinisch, B.W.; Galkin, I.A. Global ionospheric radio observatory (GIRO). Earth Planets Space 2011, 63, 377–381.

Shimazaki, T. A statistical study of occurrence probability of spread F at high latitudes. J. Geophys. Res. 1962, 67, 4617–4634. Atmosphere 2024, 15, 331 17 of 17 34.

Tiwari, R., Strangeways, H.J., Tiwari, S., & Ahmed, A. (2013). Investigation of ionospheric irregularities and scintillation using TEC at high latitude. *Advances in Space Research, 52*(6), 1111–1124.

Tsunoda, R. T. (1985). Control of the seasonal and longitudinal occurrence of equatorial scintillations by the longitudinal gradient in integrated E region Pedersen conductivity. Journal of Geophysical Research: Space Physics, 90(A1), 447–456.

Vadakke Veettil, S., Haralambous, H., & Aquino, M. (2017). Observations of quiet-time moderate mid-latitude L-band scintillation in association with plasma bubbles. *GPS Solutions, 21*(3), 1113–1124.

Wang, Z., Shi, J.K., Torkar, K., Wang, G.J., & Wang, X. (2014). Correlation between ionospheric strong range spread F and scintillations observed in Vanimo station. *Journal of Geophysical Research: Space Physics, 119*(10), 8578–8585.

Yang, Z.; Liu, Z. Correlation between ROTI and Ionospheric Scintillation Indices using Hong Kong low-latitude GPS data. GPS Solut. 2016, 20, 815–824.

Ye, H.; Yi, W.; Zhou, B.; Wu, J.; Yu, B.; Tian, P.; Wang, J.; Long, C.; Lu, M.; Xue, X.; et al. Multi-Instrumental Observations of Mid-latitude Plasma Irregularities over Eastern Asia during a Moderate Magnetic Storm on 16 July 2003. Remote Sens. 2023, 15, 1160.

Yokoyama, T.; Hysell, D.L.; Otsuka, Y.; Yamamoto, M. Three-dimensional simulation of the coupled Perkins and Es-layer instabilities in the nighttime mid-latitude ionosphere. J. Geophys. Res. Space Phys. 2009, 114.

Zakharenkova, I., Astafyeva, E., & Cherniak, I. (2020). Ionospheric irregularities and scintillations during geomagnetic storms: Role of the auroral oval expansion. Space Weather, 18(6), e2020SW002503. https://doi.org/10.1029/2020SW002503.

Zhang, S., Liu, J.Y., Yue, J., and Zhao, B., 2015. Longitudinal and seasonal variation of ionospheric disturbances. Journal of Geophysical Research: Space Physics, 120(7), pp. 6443-6462.